Relativistic many-body calculations of excitation energies, line strengths, transition rates, and oscillator strengths in Pd-like ions

U.I. Safronova, T.E. Cowan, and W. R. Johnson

Abstract: Excitation energies, line strengths, oscillator strengths, and transition probabilities are calculated for $4d^{-1}4f$, $4d^{-1}5p$, $4d^{-1}5f$, and $4d^{-1}6p$ hole–particle states in Pd-like ions with nuclear charges Z ranging from 49 to 100. Relativistic many-body perturbation theory (MBPT), including the Breit interaction, is used to evaluate retarded E1 matrix elements in length and velocity forms. The calculations start from a [Kr] $4d^{10}$ closed-shell Dirac–Hartree–Fock (DHF) potential and include second- and third-order Coulomb corrections and second-order Breit–Coulomb corrections. First-order perturbation theory is used to obtain intermediate-coupling coefficients and second-order MBPT is used to determine matrix elements. Contributions from negative-energy states are included in the second-order electric-dipole matrix elements. The resulting transition energies, line strengths, and transition rates are compared with experimental values and with other recent calculations. Trends of oscillator strengths as functions of nuclear charge Z are shown graphically for all transitions from the $4d^{-1}4f$, $4d^{-1}5p$, $4d^{-1}5f$, and $4d^{-1}6p$ states to the ground state.

PACS Nos.: 31.15.Ar, 31.15.Md, 32.70.Cs, 32.30.Rj, 31.25.Jf

Résumé : Nous calculons les énergies d'excitation, les intensités de ligne, les forces d'oscillateur et les probabilités de transition pour les états $4d^{-1}4f$, $4d^{-1}5p$, $4d^{-1}5f$ et $4d^{-1}6p$ dans les ions de type Pd avec charge nucléaire allant de $Z = 49$ à 100. Nous utilisons une méthode relativiste de perturbations à N-corps (MBPT), incluant l'interaction de Breit, afin d'évaluer les éléments de matrice E1 retardés sous les formes longueur et moment. Le calcul démarre avec un potentiel de Dirac–Hartree–Fock pour couche $4d^{10}$ [Kr] fermée et comprend les corrections de Coulomb aux deuxième et troisième ordres et les corrections de Breit–Coulomb au deuxième ordre. La théorie des perturbations au premier ordre est utilisée pour obtenir les coefficients de couplage intermédiaire et MBPT au deuxième ordre sert à calculer les éléments de matrice. Nous incluons les contributions des états d'énergie négative dans le calcul au deuxième ordre des éléments de matrice du dipôle électrique. Nous comparons les énergies de transition, les intensités de ligne et les taux de transition avec des valeurs expérimentales et avec d'autres calculs récents. Nous montrons graphiquement

Received 9 March 2005. Accepted 25 May 2005. Published on the NRC Research Press Web site at http://cjp.nrc.ca/ on 14 July 2005.

U.I. Safronova[1] and T.E. Cowan. Physics Department, University of Nevada, Reno, NV 89557, USA.
W. R. Johnson. Department of Physics, University of Notre Dame, Notre Dame, IN 46566, USA.

[1]Corresponding author (e-mail: usafrono@nd.edu). On leave from ISAN, Troitsk, Russia.

 doi: 10.1139/P05-036

les tendances des forces d'oscillateur en fonction de la charge nucléaire pour toutes les transitions des états $4d^{-1}4f$, $4d^{-1}5p$, $4d^{-1}5f$ et $4d^{-1}6p$ vers le fondamental.

[Traduit par la Rédaction]

1. Introduction

Relativistic many-body perturbation theory (MBPT) studies of hole–particle excitations of closed-shell ions were performed by Avgoustoglou and co-workers [1–4] for Ne-like ions and by Safronova and co-workers [5, 6] for Ne- and Ni-like ions. The ground states of Ne-like and Ni-like ions have completely filled $n = 1, 2$ and $n = 1, 2, 3$ shells, respectively, whereas the ground states of Pd-like ions have closed $4s$, $4p$, and $4d$ subshells and an open $4f$ subshell. In Fig. 1, we plot one-electron Dirac–Hartree–Fock (DHF) energies of the $4f$ and $5p$ states as functions of Z. As one can see from Fig. 1, the $5p$ orbitals are more tightly bound than the $4f$ orbitals at low stages of ionization while the $4f$ orbitals are more tightly bound for highly ionized cases. Competition between $4f$ and $5p$ orbitals leads to problems for MBPT, making it difficult to obtain very accurate excitation energies and line strengths for the transition between the low lying $4d^9 4f$, $4d^9 5p$, $4d^9 5f$, and $4d^9 6p$ excited states and the ground state.

Earlier line strength calculations for the $4d^{10}\,{}^1S$–$4d^9 4f\,{}^1P$ resonance transition along the palladium isoelectronic sequence were performed [7] in three approximations: configuration-averaged Hartree–Fock (HF), term-dependent HF, and MBPT. Numerical results are given in ref. 7 for three Pd-like ions, Xe^{+8}, Nd^{14+}, and W^{+28}. Relative magnitudes of the electric-multipole (E1, E2, E3) and magnetic-multipole (M1, M2, M3) radiative decay rates, calculated using the multiconfiguration DHF approach, are presented in ref. 8 for the $4d^9 4f$, $4d^9 5s$, and $4d^9 5p$ states of highly ionized Pd-like ions.

Sugar and Kaufman [9] extended the identification of the resonance lines of $4d^9 4f$ and $4d^9 5p$ configurations in the Pd I isoelectronic sequence from Nd^{+14} to Ho^{+21}. Spectra were obtained with a high-voltage spark and photographed with 10.7 m grazing incidence spectrograph. Calculations of the energy levels and eigenvectors are also made in ref. 9, including the configuration interaction between $4d^9 4f$ and $4d^9 5p$ using scaled-HF values for the radial integrals. A review of all previous identifications of resonance lines of the $4d^9 4f$ and $4d^9 5p$ configurations is also given in ref. 9. In ref. 10, the spectra of highly ionized Er, Yb, Hf, W, and Pt are observed by injecting these elements into the plasma of the TEXT tokamak at the University of Texas at Austin. Resonance lines of the $4d^{10}$–$4d^9 4f$ transition array in Pd-like ions are identified in in ref. 10 by comparison with plots of observed-minus-calculated transition energies. A detailed analysis of the various transitions in Pd-like ions was performed by Churlikov et al. [11–15]. To predict the $4d^{10}$–$4d^9(np + n'f)$ transitions in Cd III–Cs X, relativistic HF calculations using the Cowan code with scaling are completed in ref. 11. The $4d^9 5l$–$4d^9 5l'$ spectra in Pd-like ions Sb VI, Te VII, and I VIII were investigated in the 400–900 Å region using vacuum spark sources [12]. Experimental results for $4d^9 5s$, $4d^9 5d$, and $4d^9 5p$ states in CsX–Ce XIII ions are obtained in ref. 14 with the aid of high-resolution spectrographs supplemented by theoretical calculations made using the Cowan code and by fitting with orthogonal operator techniques. It is emphasized in ref. 14 that ions of the palladium isoelectronic sequence are currently of interest for the development of extreme-ultraviolet (XUV) lasers.

High-resolution spectra of xenon ions from Xe IX to Xe XIV at 95–155 Å are presented in ref. 15. In the region of importance for XUV lithography (near 134 Å) the strongest lines were identified as $4d^8$–$4d^7 5p$ transitions in Xe XI. The most intense lines in Xe IX were found to be the $4d^{10}\,{}^1S_0 - 4d^9 4f\,{}^1P_1$ line at 120.135 Å and the $4d^{10}\,{}^1S_0 - 4d^9 4f\,{}^3D_1$ line at 143.614 Å.

In the present paper, relativistic many-body perturbation theory is used to determine energies of Pd-like ions. Second-order MBPT calculations for Pd-like ions start from a [Kr] $4d^{10}$ DHF potential. Third-order one-body Coulomb contributions are also included in the present calculation and found to significantly improve the agreement between calculation and measurement. We consider $4d$ holes and

Fig. 1. One-electron DHF energies ($E/(Z-35)^2$ in cm^{-1}) of $4f_j$ and $5p_j$ states as functions of Z.

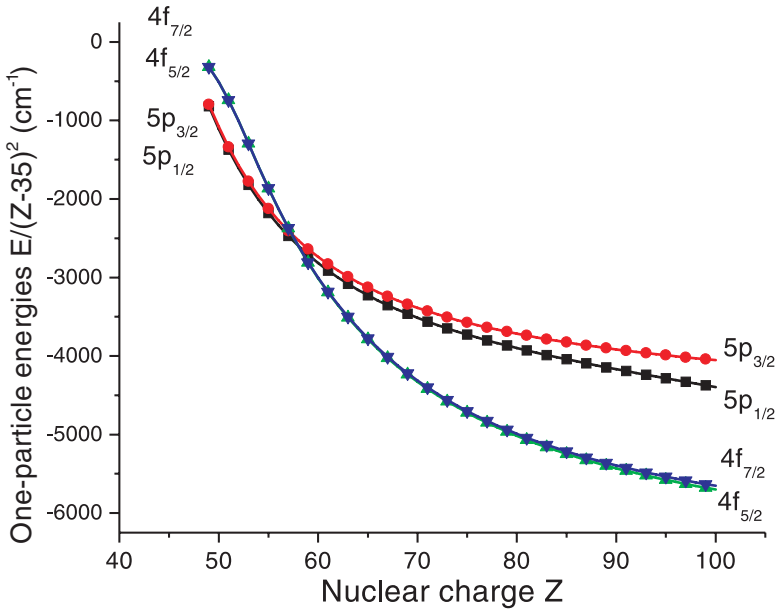

$4f$, $5p$, $5f$, and $6p$ particles leading to 12 odd-parity $4d^{-1}nl'[J]$ states with $J = 1$. We calculate the energies of these 12 states for ions with nuclear charge $Z = 49$–100.

Relativistic MBPT is also used to determine reduced matrix elements, line strengths, oscillator strengths, and transition rates for electric dipole transitions from the $4d^9nl'$ states to the $4d^{10}\,{}^1S_0$ ground state in Pd-like ions. Retarded E1 matrix elements are evaluated in both length and velocity forms. The MBPT calculations start from a nonlocal [Kr] $4d^{10}$ DHF potential and consequently give gauge-dependent transition matrix elements. Second-order correlation corrections compensate almost exactly for the gauge dependence of the first-order matrix elements, leading to corrected matrix elements that differ by less than 5% in length and velocity forms throughout the isoelectronic sequence. A detailed breakdown of contributions to energies and transition matrix elements for the case of Xe^{+8} is given in Appendices A and B, respectively.

2. Second-order MBPT calculations of energies of Pd-like ions

Details of the MBPT method are presented in refs. 1 and 6 for the calculation of energies of hole–particle states, in ref. 16 for the calculation of energies of particle–particle states, in ref. 17 for the calculation of radiative electric-dipole rates in two-particle states, and in ref. 5 for the calculation of multipole radiative rates in hole–particle states. Here, we present only the model space for Pd-like ions without repeating the detailed discussions given in refs. 1, 5, 6, 16, 17. Differences between the calculations for Ni- and Pd-like ions arise because of the increased number of the core orbitals in the DHF potential ($1s^22s^22p^63s^23p^63d^{10}4s^24p^64d^{10}$ instead of $1s^22s^22p^63s^23p^63d^{10}$) and the strong mixing between odd-parity states ($4d^{-1}4f + 4d^{-1}5p$). These differences lead to much more laborious numerical calculations. The calculations are carried out using a finite basis set of DHF orbitals. The orbitals used in the present calculation are obtained as linear combinations of B-splines. The B-spline basis orbitals are calculated using the method described in ref. 18. We use 40 B-splines of order 7 for each single-particle angular momentum state and we include all orbitals with orbital angular momentum $l \leq 9$ in our basis.

Table 1. $J = 1$ hole–particle states in the $4djnl'j'$ complex for Pd-like ions in jj and LS coupling schemes.

jj	LS	jj	LS
$4d_{5/2}5p_{3/2}\,[1]$	$4d5p\,^3P_1$	$4d_{5/2}6p_{3/2}\,[1]$	$4d6p\,^3P_1$
$4d_{3/2}5p_{1/2}\,[1]$	$4d5p\,^1P_1$	$4d_{3/2}6p_{1/2}\,[1]$	$4d6p\,^1P_1$
$4d_{3/2}5p_{3/2}\,[1]$	$4d5p\,^3D_1$	$4d_{3/2}6p_{3/2}\,[1]$	$4d6p\,^3D_1$
$4d_{5/2}4f_{5/2}\,[1]$	$4d4f\,^3P_1$	$4d_{5/2}5f_{5/2}\,[1]$	$4d5f\,^3P_1$
$4d_{5/2}4f_{7/2}\,[1]$	$4d4f\,^3D_1$	$4d_{5/2}5f_{7/2}\,[1]$	$4d5f\,^3D_1$
$4d_{3/2}4f_{5/2}\,[1]$	$4d4f\,^1P_1$	$4d_{3/2}5f_{5/2}\,[1]$	$4d5f\,^1P_1$

2.1. Model space

For atoms with one hole in closed shells and one particle above closed shells, the model space is formed from hole–particle states of the type $a_v^\dagger a_a|0\rangle$, where $|0\rangle$ is the [Kr] $4d_{3/2}^4 4d_{5/2}^6$ ground state. The operators a_a and $a_v^\dagger$ are core annihilation and particle creation operators, respectively. Particle indices v range over states in the valence shell and hole indices and particle indices a range over the closed core. In our study of low-lying $4d^{-1}nl$ states of Pd-like ions, values of a are limited to $4d_{3/2}$ and $4d_{5/2}$, while values of v are $4f_{5/2}$, $4f_{7/2}$, $5p_{1/2}$, $5p_{3/2}$, $5f_{5/2}$, $5f_{7/2}$, $6p_{1/2}$, and $6p_{3/2}$. The hole and particle states can be combined to give 12 odd-parity states with $J = 1$. These states are listed in Table 1, where both jj and LS designations are given. Note that LS labeling is used in all of the references mentioned previously [9–15], even though the LS-coupling description is most appropriate for low stages of ionization. For simplicity, we replace the $4d_j^{-1}nl_{j'}$ or $4d^{-1}nl$ designations by $4d_jnl_{j'}$ or $4dnl$ in Table 1 and in all of the following tables and text.

We have already mentioned that there is strong mixing between the $4d4f$ and $4d5p$ states. In Fig. 2, we illustrate the contribution of these states to the $4d5p\,^3P_1$ level in the interval $Z = 49$–100. For $Z = 49$–53, the largest contribution to the $4d5p\,^3P_1$ level is from the $4d_{5/2}5p_{3/2}\,[1]$ state. The $4d_{3/2}5p_{1/2}\,[1]$ state dominates for $Z = 54$–55 and, for $Z > 56$, the $4d_{5/2}4f_{5/2}\,[1]$ state contributes about 90% to the $4d5p\,^3P_1$ level. The same strong mixing affects the $4d5p\,^1P_1$ and $4d5p\,^3D_1$ levels. From Fig. 2, it is obvious that the LS labeling $4d4p\,^3P_1$ given in Table 1 is meaningful only for low stages of ionization; starting from $Z = 58$ the dominant contribution to this state is from the $4d_{5/2}5f_{5/2}\,[1]$ configuration.

2.2. Z dependence of energies in Pd-like ions

In Fig. 3, we illustrate the Z dependence of the second-order energy corrections $E^{(2)}$ for $4d4f\,^3P_1$, $^3D_1$, $^1P_1$ and $4d5f\,^3P_1$, $^3D_1$, $^1P_1$ states in Pd-like ions. The second-order energy $E^{(2)}$ is a smooth function of Z for $4d4f$ and $4d5p$ configurations, but exhibits a few sharp features for $4d5f$ configurations. These very strong irregularities occur for the $4d5f\,^3P_1$ state ($Z = 81$, 89), $4d5f\,^3D_1$ state ($Z = 64$, 79, 81, 88), and $4d5f\,^1P_1$ state ($Z = 81$, 89) and are explained by vanishing energy denominators in MBPT expressions for correlation corrections. We give some numerical details relevant to this issue in Appendix C.

Energies of the $J = 1$ $4d4f$ and $4d5p$ states relative to the ground state are shown in Fig. 4. We plot the six energy levels within the odd-parity $J = 1$ complex that are involved in the mixing of states illustrated in Fig. 2. It was already shown that the largest mixing coefficient contributing to the $4d5p\,^3P_1$ level is different for $Z \leq 54$ and $Z \geq 55$. This change can also be observed in Fig. 4. The first ($4d5p\,^3P_1$) and fourth ($4d4f\,^3P_1$) level curves cross for $Z = 55$. The difference $E[4d5p\,^3P_1] - E[4d4f\,^3P_1]$ at $Z = 55$ is just 4% of the energy $E[4d5p\,^3P_1]$. A similar Z dependence and strong mixing for these levels was found by the authors of ref. 9.

Fig. 2. Mixing coefficients as functions of Z for odd-parity states with $J = 1$ in Pd-like ions.

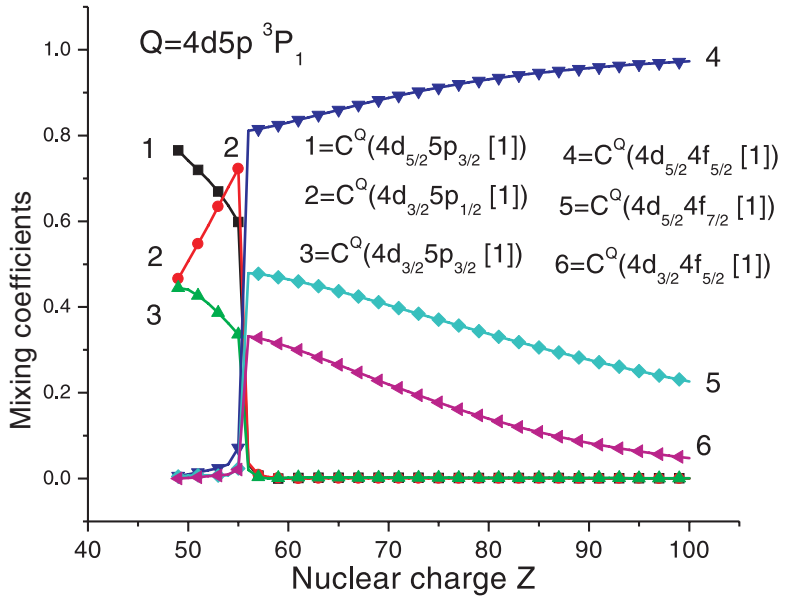

Fig. 3. Second-order Coulomb energies as functions of Z for $4d4f$ and $4d5f$ states with J=1 in Pd-like ions.

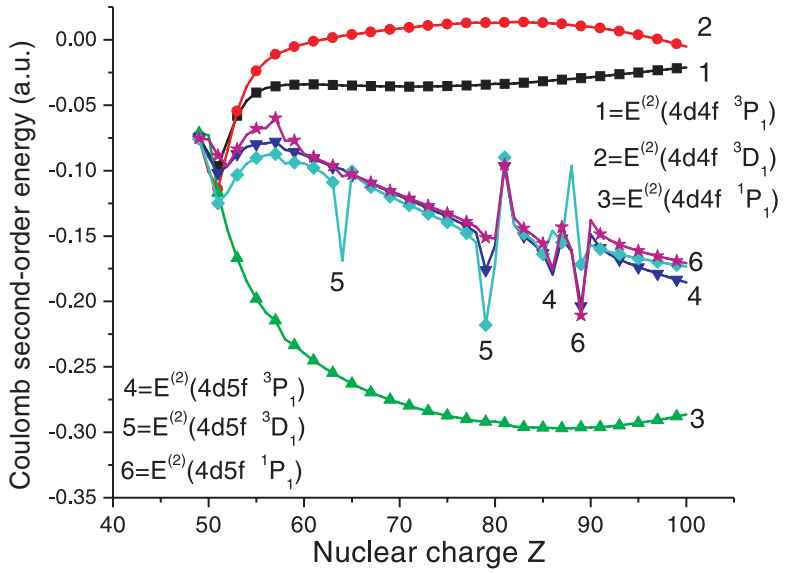

3. Third-order MBPT contribution to energies of Pd-like ions

The importance of third-order contributions in obtaining precise energies for Li-, Na-, Cu-, and Ag-like ions is established in refs. 19–22. Moreover, large third-order contributions for $4f_{5/2}$ and $4f_{7/2}$ states in Ce IV and Pr V were found recently in ref. 23 where third-order energies for $4f$ states were found to be about 35% of second-order energies.

Results of the present third-order calculations for energies of $4f$ and $5p$ particle states, which are

Fig. 4. Excitation energies $(E/(Z-35)^2)$ in cm^{-1} for $4d4f$ and $4d5p$ states with $J = 1$ as functions of Z.

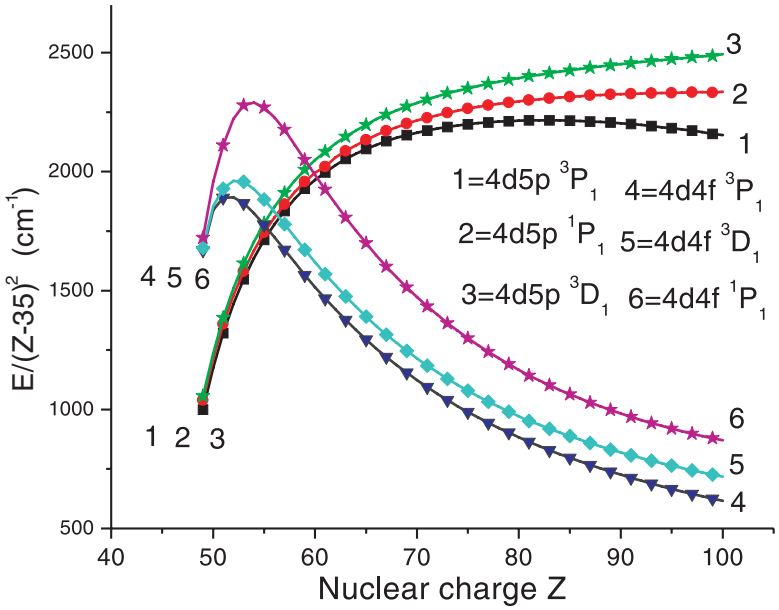

Fig. 5. Second- and third-order particle contributions to energies in Pd-like ions.

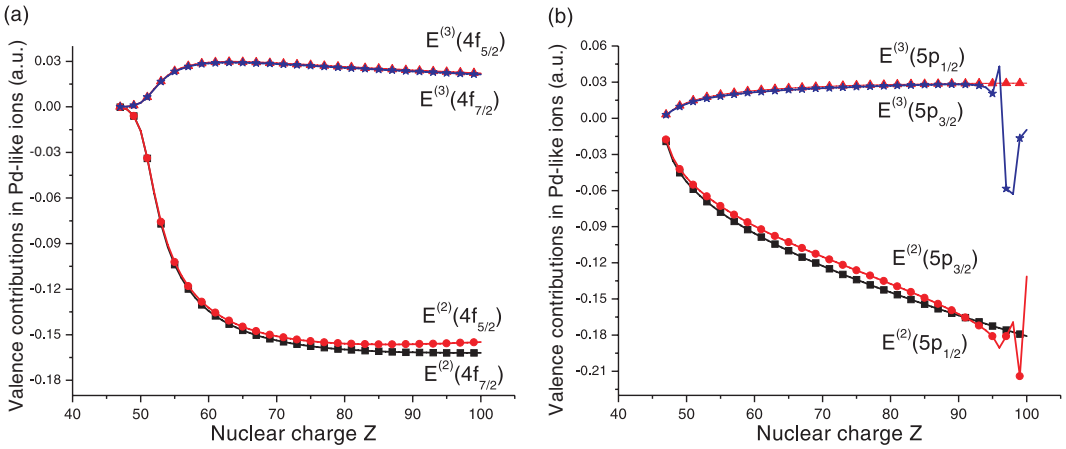

evaluated as described in ref. 22, are shown in Fig. 5, where we compare second- and third-order contributions. We compare $E^{(3)}$ and $E^{(2)}$ for $4d$ hole states in Fig. 6. We see from these figures that $E^{(3)}$ and $E^{(2)}$ have different signs; consequently, third-order contributions substantially decrease the magnitude of the correlation correction. Values of $E^{(3)}(4f)$ and $E^{(3)}(5p)$ slowly increase with increasing Z, whereas the value of $E^{(3)}(4d)$ decreases with increasing Z.

We include both the one- and two-body contributions to the second-order energy, but only the one-body contribution to the third-order energy in the present work. Indeed, we find that the two-body contribution to $E^{(2)}$ is smaller in magnitude than the one-body contribution by a factor of 2–5. In Fig. 7, the second-order energy is compared with the combined second- and third-order energy. The data presented in Fig. 7 are obtained by diagonalizing the energy matrix within the $4d4f$ model space.

Fig. 6. Second- and third-order hole contributions to energies in Pd-like ions.

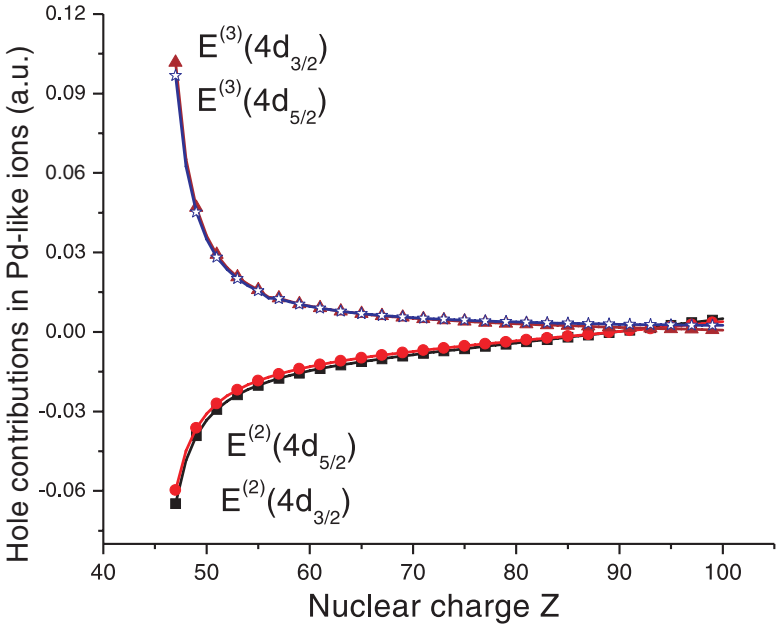

Fig. 7. Coulomb contributions to the energies as functions of Z for $4d4f$ states with $J = 1$ in Pd-like ions.

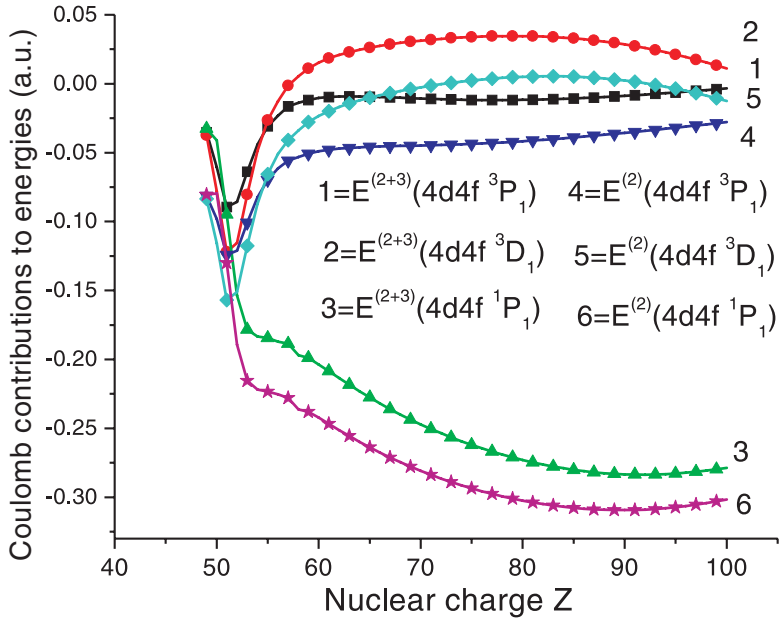

Differences between second-order values and second-order + third-order values are seen to be almost constant and equal to 0.03–0.04 a.u.

Results of our relativistic many-body perturbation theory in second- and third-order MBPT (labeled

MBPT2 and MBPT3) are given in Table 2. In Table 2, we compare our results for energy levels of the three hole–particle $4d4f$ states of interest in Pd-like ions with the experimental measurements given in refs. 9–11, 13. Although our results are generally in good agreement with experimental data, discrepancies were found. One cause for these discrepancies is the omission of two-body third-order correlation corrections. However, we have no explanation for the increasing discrepancy found in the $4d4f\,^1P_1$ level with the increasing Z; 680 cm^{-1} for $Z = 65$, 1400 cm^{-1} for $Z = 66$, and 17 900 cm^{-1} for $Z = 78$.

4. Electric-dipole matrix elements

In the following paragraphs, we present electric-dipole (E1) matrix elements for transitions between the odd-parity $J = 1$ states belonging to the $4d_j4f_{j'}[1]$, $4d_j5f_{j'}[1]$, $4d_j5p_{1/2}[1]$, and $4d_j6p_{j'}[1]$ configurations and the ground state for Pd-like ions. Analytical expressions for E1 matrix elements in second-order MBPT are given in ref. 6 and will not be repeated here. The first- and second-order Coulomb–Breit corrections to E1 matrix elements are referred to as $Z^{(1)}$, $Z^{(2)}$, and $B^{(2)}$, respectively, in the text below. These contributions are calculated in both length and velocity forms, and include contributions from negative energy states.

5. Oscillator strengths, transition rates, and line strengths

Oscillator strengths for the 12 E1 lines from ($4d4f\ ^3P_1$, $^3D_1$, $^1P_1$), ($4d5f\ ^3P_1$, $^3D_1$, $^1P_1$), ($4d5p\ ^3P_1$, $^1P_1$, $^3D_1$), and ($4d6p\ ^3P_1$, $^1P_1$, $^3D_1$) levels to the ground state are plotted in Fig. 8. The sharp features in the curves shown in Fig. 8 are explained in many cases by strong mixing of states inside of the odd-parity complex with $J = 1$.

The deep minimum in the curves labeled $4d4f\,^3P_1$, ($Z = 88$), $4d5f\,^3P_1$, ($Z = 92$), and $4d5p\,^3P_1$ ($Z = 56$) are due to mixing of the $[4d_{5/2}4f_{5/2}\,[1] + 4d_{5/2}4f_{7/2}\,[1]]$, $[4d_{5/2}5f_{5/2}\,[1] + 4d_{5/2}5f_{7/2}\,[1]]$, and $[4d_{3/2}5p_{1/2}\,[1] + 4d_{5/2}5p_{3/2}\,[1]]$ states, respectively. It should be noted that the mixing of those states is not very large (about 15–20%) in the first two cases; however, the ratios of dipole-matrix elements, $Z^{(1+2)}(0 - 4d_{5/2}4f_{7/2}\,[1])$ and $Z^{(1+2)}(0 - 4d_{5/2}4f_{5/2}\,[1])$ as well as matrix elements, $Z^{(1+2)}(0 - 4d_{5/2}5f_{7/2}\,[1])$ and $Z^{(1+2)}(0 - 4d_{5/2}5f_{5/2}\,[1])$ are equal to 4–5 (see Table B.1) and the sign of these ratios is different from the sign of the corresponding ratio of mixing coefficients. This leads to cancellation since the coupled matrix elements are a product of matrix elements and mixing coefficients. As a result, deep minima occur in the curves $4d4f\,^3P_1$ at $Z = 88$ and $4d5f\,^3P_1$ at $Z = 92$.

Singularities in the curves labeled $4d6p\,^3P_1$, $^1P_1\,^3D_1$ have a different origin. We found a sharp increase in the second-order RPA contributions for $Z = 57$ ($4d_{3/2}6p_{1/2}$) and for $Z = 61$, 67, and 79 ($4d_{5/2}6p_{3/2}$) resulting from very small energy denominators. As a result, the second-order contribution becomes very large, leading to deviations from the smooth curves in Fig. 8. Details are given in Appendix D.

In Table 3, we compare our MBPT values of E1 transition rates with theoretical results of ref. 8. We list results for transitions between $4d4f$ and $4d5p$ excited states and the ground state for selected ions ($Z = 92$, 90, 80, and 70). The differences between our results and those from ref. 8 range from 0–10% for $4d5p\,^3P_1$, $^1P_1$ levels and 30–40% for $4d4f\,^3P_1$, $^3D_1$, $^1P_1$ and $4d5p\,^3D_1$ levels. These differences are the result of the different computational methods used; the present results are from second-order MBPT calculations while results in ref. 8 were obtained using the MCDF approximation. Second-order contributions to matrix elements, which are relatively large, are illustrated for Xe^{+8} in Table B.2 of Appendix B where we compare first- and second-order MBPT values. The fact that correlation corrections to matrix elements in Pd-like ions are large was also noted in ref. 7.

In Table 4, we compare our MBPT results for line strengths $S^{(1)}$ and $S^{(1+2)}$ with theoretical results $S_{\rm HF}$ and $S_{\rm MBPT}$ from ref. 7. In particular, we list results for the transition between the $4d4f\,^1P_1$ excited state and the ground state for nine ions from $Z = 50$ to 74 presented in ref. 7. It should be noted that

Table 2. Excitation energies (in cm^{-1}) for $4d4f$ states in Pd-like ions calculated in MBPT2 and MBPT3 approximation.

Z	Ion	$^3P_1$	$^3D_1$	$^1P_1$	Z	Ion	$^3P_1$	$^3D_1$	$^1P_1$
49	MBPT2	329 175	330 205	338 330	64	MBPT2	1 122 793	1 200 753	1 472 547
	MBPT3	339 295	340 331	348 834		MBPT3	1 130 887	1 208 834	1 480 606
	Expt.	328 552[a]	333 968[a]	343 006[a]		Expt.		1 200 200[c]	1 478 500[c]
50	MBPT2	417 464	419 175	440 551	65	MBPT2	1 165 730	1 248 112	1 528 313
	MBPT3	425 733	427 500	449 023		MBPT3	1 173 718	1 256 082	1 536 262
	Expt.	412 316[a]	423 372[a]	446 348[a]		Expt.	1 183 500[c]	1 246 900[c]	1 535 580[c]
51	MBPT2	488 162	492 090	538 076	66	MBPT2	1 208 368	1 295 305	1 583 669
	MBPT3	495 775	499 774	545 783		MBPT3	1 217 240	1 303 164	1 591 509
	Expt.	485 458[a]	502 840[a]	547 063[a]		Expt.		1 294 600[c]	1 592 900[c]
52	MBPT2	548 489	560 104	636 538	67	MBPT2	1 250 745	1 342 393	1 638 735
	MBPT3	556 247	567 918	644 346		MBPT3	1 258 520	1 350 141	1 646 465
	Expt.	550 113[a]	573 155[a]	649 003[a]		Expt.			1 649 500[c]
53	MBPT2	605 122	626 451	734 487	68	MBPT2	1 292 892	1 389 426	1 693 611
	MBPT3	613 232	634 606	742 624		MBPT3	1 300 563	1 397 065	1 701 232
	Expt.	609 143[a]	636 983[a]	744 596[a]		Expt.		1 388 100[d]	1 706 200[d]
54	MBPT2	659 075	688 918	825 331	69	MBPT2	1 334 839	1 436 454	1 748 384
	MBPT3	667 463	697 343	833 731		MBPT3	1 342 407	1 443 984	1 755 897
	Expt.	665 450[b]	696 310[b]	832 410[b]		Expt.			
55	MBPT2	710 670	747 434	907 529	70	MBPT2	1 376 609	1 483 514	1 803 129
	MBPT3	719 227	756 021	916 089		MBPT3	1 384 076	1 490 938	1 810 537
	Expt.	716 673[a]	752 513[a]	912 500[a]		Expt.			1 818 300[d]
56	MBPT2	760 405	802 939	982 632	71	MBPT2	1 418 222	1 530 645	1 857 916
	MBPT3	768 786	811 345	991 010		MBPT3	1 425 590	1 537 965	1 865 220
	Expt.		806 445[c]	986 280[c]		Expt.			
57	MBPT2	808 685	856 225	1 052 467	72	MBPT2	1 459 699	1 577 880	1 912 804
	MBPT3	817 330	864 890	1 061 104		MBPT3	1 466 970	1 585 097	1 920 007
	Expt.		856 201[c]	1 055 253[b]		Expt.			1 930 400[d]
58	MBPT2	855 552	907 801	1 117 388	73	MBPT2	1 501 053	1 625 249	1 967 851
	MBPT3	864 167	916 432	1 125 991		MBPT3	1 508 229	1 632 365	1 974 954
	Expt.		909 512[c]	1 120 610[c]		Expt.			
59	MBPT2	901 636	958 429	1 180 977	74	MBPT2	1 542 300	1 672 779	2 023 109
	MBPT3	910 195	966 999	1 189 519		MBPT3	1 549 385	1 679 798	2 030 115
	Expt.		959 462[c]	1 183 540[c]		Expt.		1 670 800	2 043 000
60	MBPT2	946 988	1 008 024	1 241 899	75	MBPT2	1 583 452	1 720 497	2 078 627
	MBPT3	955 472	1 016 514	1 250 362		MBPT3	1 590 447	1 727 420	2 085 537
	Expt.		1 008 580[c]	1 242 950[c]		Expt.			
61	MBPT2	991 684	1 056 908	1 301 162	76	MBPT2	1 624 521	1 768 425	2 134 452
	MBPT3	1 000 090	1 065 315	1 309 544		MBPT3	1 631 428	1 775 255	2 141 269
	Expt.					Expt.			
62	MBPT2	1 035 830	1 105 244	1 359 173	77	MBPT2	1 665 517	1 816 587	2 190 629
	MBPT3	1 044 130	1 113 540	1 367 445		MBPT3	1 672 339	1 823 326	2 197 355
	Expt.		1 105 100[c]	1 361 200[c]		Expt.			
63	MBPT2	1 079 511	1 153 158	1 416 226	78	MBPT2	1 706 448	1 865 001	2 247 202
	MBPT3	1 087 710	1 161 348	1 424 393		MBPT3	1 713 187	1 871 651	2 253 839
	Expt.	1 096 700[c]	1 152 800	1 420 370[c]		Expt.			2 271 700[d]

[a]Experimental measurements performed in ref. 11.
[b]Experimental measurements performed in ref. 13.
[c]Experimental measurements performed in ref. 9.
[d]Experimental measurements performed in ref. 10.

Fig. 8. Oscillator strengths for transitions between the ground state and $4d4f$, $4d5f$, $4d5p$, and $4d6p$ states as functions of Z.

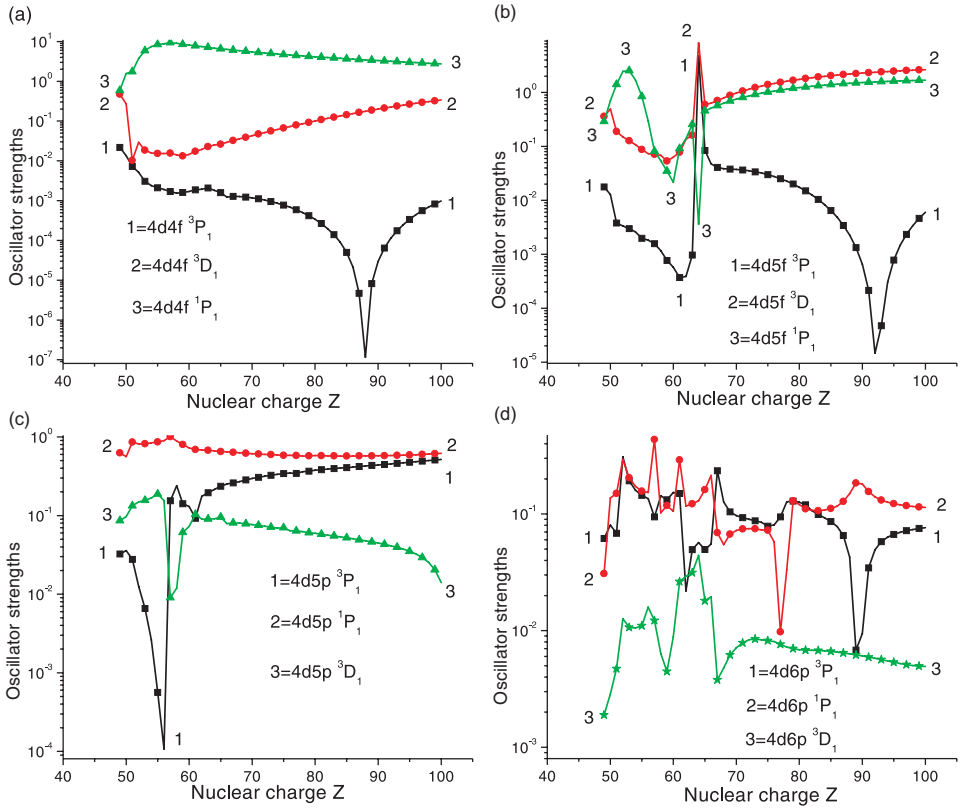

Table 3. Transition rates (A_r in s^{-1}) in Pd-like ions for transitions between excited $4d4f\,^3P_1$, $^3D_1$, $^1P_1$, $4d5p\,^3P_1$, $^1P_1$, $^3D_1$, states and the ground state. Comparison of (*a*) the present MBPT results with (*b*) the theoretical results from ref. 8.

		A_r (s^{-1})			
Level		$Z = 92$	$Z = 90$	$Z = 80$	$Z = 70$
$4d4f\,^3P_1$	(*a*)	1.30 [08]	3.18 [07]	2.43 [08]	5.02 [08]
$4d4f\,^3D_1$	(*a*)	3.31 [11]	2.70 [11]	8.54 [10]	2.10 [10]
	(*b*)	4.47 [11]	3.66 [11]	1.18 [11]	2.92 [10]
$4d4f\,^1P_1$	(*a*)	7.11 [12]	6.80 [12]	5.41 [12]	4.24 [12]
	(*b*)	9.47 [12]	9.09 [12]	7.32 [12]	5.74 [12]
$4d5p\,^3P_1$	(*a*)	5.16 [12]	4.37 [12]	1.70 [12]	4.68 [11]
	(*b*)	5.50 [12]	4.66 [12]	1.81 [12]	5.01 [11]
$4d5p\,^1P_1$	(*a*)	7.42 [12]	6.37 [12]	2.80 [12]	1.01 [12]
	(*b*)	6.75 [12]	5.87 [12]	2.69 [12]	1.01 [12]
$4d5p\,^3D_1$	(*a*)	5.91 [11]	5.50 [11]	3.12 [11]	1.36 [11]
	(*b*)	7.78 [11]	6.90 [11]	3.54 [11]	1.28 [11]

the results for nine ions in ref. 7 were obtained only in the HF approximation S_{HF}. The MBPT results in ref. 7 were given only for three ions, $Z = 54$, 60, and 74. Our MBPT results, $S^{(1+2)}$ and those from [7] S_{MBPT} agree surprisingly well (1%, and 2% for ions with $Z = 60$, and 74, respectively.

Table 4. Line strengths (S in a.u.) in Pd-like ions for transitions between excited $4d4f\,^1P_1$ states and the ground state. Comparison of our first-order $S^{(1)}$ and second-order $S^{(1+2)}$ line strengths with theoretical results (^{a}) from ref. 7.

Ion	$S^{(1)}$	$S^{(1+2)}$	$S^a_{\rm HF}$	$S^a_{\rm MBPT}$
Sn VII	1.611	1.129	1.445	
Te VII	3.167	1.843	2.599	
I VIII	3.574	2.504	3.180	
Xe IX	3.803	2.853	3.579	2.36
Cs X	3.804	2.920	3.701	
Ba XI	3.648	2.803	3.593	
Nd XV	2.683	2.063	2.606	2.079
Ho XXII	1.575	1.182	1.514	
W XXIX	1.022	0.766	0.9834	0.7512

6. Conclusion

In summary, a systematic second-order MBPT study of excitation energies of the 12 $4d^{-1}4f$, $4d^{-1}5p$, $4d^{-1}5f$, and $4d^{-1}6p$ hole–particle states of Pd-like ions has been presented. Theoretical excitation energies of Pd-like ions In^{3+}–Pt^{32+} differ from existing experimental wavelengths data at the level of 0.01–2.0%.

We also presented a systematic second-order relativistic MBPT study of reduced matrix elements, line strengths, oscillator strengths, and transition rates for electric-dipole transitions into the ground state in Pd-like ions with nuclear charges ranging from $Z = 49$ to 100. The reduced dipole matrix elements include correlation corrections from Coulomb and Breit interactions. Both length and velocity forms of the matrix elements were evaluated, and small differences, caused by the nonlocality of the starting DHF potential, were found between the two forms. Second-order MBPT transition energies were used to evaluate oscillator strengths and transition rates. We believe that our results will be useful in analyzing existing experimental data and in planning new experiments.

Acknowledgments

The work of W.R.J. was supported in part by the National Science Foundation Grant No. PHY-01-39928. The work of T.E.C. and U.I.S. was supported by DOE/NNSA under UNR grant DE-FC52-01NV14050. U.I.S. would like to thank M.S. Safronova for helpful discussions.

References

1. E. Avgoustoglou, W.R. Johnson, D.R. Plante, J. Sapirstein, S. Sheinerman, and S.A. Blundell. Phys. Rev. A, **46**, 5478 (1992).
2. E. Avgoustoglou, W.R. Johnson, and J. Sapirstein. Phys. Rev. A, **51**, 1196 (1995).
3. E. Avgoustoglou and Z.W. Liu. Phys. Rev. A, **54**, 1351 (1996).
4. E.N. Avgoustoglou and D.R. Beck. Phys. Rev. A, **57**, 4286 (1998).
5. U.I. Safronova, C. Namba, I. Murakami, W.R. Johnson, and M.S. Safronova. Phys. Rev. A, **64**, 012517 (2001).
6. U.I. Safronova, W.R. Johnson, and J. Albritton. Phys. Rev. A, **62**, 052505 (2000).
7. S.M. Younger. Phys. Rev. A, **22**, 2682 (1980).
8. E. Biémont. J. Phys. B, **30**, 4207 (1997).
9. J. Sugar and V. Kaufman. Phys. Scr. **26**, 419 (1982).

10. J. Sugar and V. Kaufman. J. Opt. Soc. Am. B, **10**, 799 (1993).
11. S.S. Churilov, Y.N. Joshi, and A.N. Ryabtsev. J. Phys. B, **27**, 5485 (1994).
12. S.S. Churilov, V.A. Azarov, A.N. Ryabtsev, W.-Ü.L. Tchang-Brillet, and J.-F. Wyart. Phys. Scr. **61**, 420 (2000).
13. S.S. Churilov, A.N. Ryabtsev, W.-Ü.L. Tchang-Brillet, and J.-F. Wyart. Phys. Scr. **65**, 40 (2002).
14. S.S. Churilov and Y.N. Joshi. Phys. Scr. T, **100**, 98 (2002).
15. S. Churilov, Y.N. Joshi, and J. Reader. Opt. Lett. **28**, 1478 (2003).
16. M.S. Safronova, W.R. Johnson, and U.I. Safronova. Phys. Rev. A, **53**, 4036 (1996).
17. U.I. Safronova, W.R. Johnson, M.S. Safronova, and A. Derevianko. Phys. Scr. **59**, 286 (1999).
18. W.R. Johnson, S.A. Blundell, and J. Sapirstein. Phys. Rev. A, **37**, 2764 (1988).
19. W.R. Johnson, S.A. Blundell, and J. Sapirstein. Phys. Rev. A, **37**, 2794 (1988).
20. W.R. Johnson, S.A. Blundell, and J. Sapirstein. Phys. Rev. A, **38**, 2699 (1988).
21. W.R. Johnson, S.A. Blundell, and J. Sapirstein. Phys. Rev. A, **42**, 1087 (1990).
22. U.I. Safronova, I.M. Savukov, M.S. Safronova, and W.R. Johnson. Phys. Rev. A, **68**, 062505 (2003).
23. I.M. Savukov, W.R. Johnson, U.I. Safronova, and M.S. Safronova. Phys. Rev. A, **67**, 042504 (2003).
24. M.H. Chen, K.T. Cheng, and W.R. Johnson. Phys. Rev. A, **47**, 3692 (1993).

Appendix A. Energy matrix for Xe^{+8}

In Table A.1, we list contributions to the second-order energies for the special case of Pd-like xenon, $Z = 54$. In the table, we give the one-body and two-body second-order Coulomb contributions to the energy matrix labeled $E_1^{(2)}$ and $E_2^{(2)}$, respectively. The corresponding Breit–Coulomb contributions are listed in columns headed $B_1^{(2)}$ and $B_2^{(2)}$. The one-body second-order energy is a sum of the valence and hole energies; the later being the dominant contribution [6]. The values of $E_1^{(2)}$ and $B_1^{(2)}$ are nonzero only for diagonal matrix elements. There are 12 diagonal and 60 nondiagonal matrix elements for $4d_j nl_{j'}$ [1] hole–particle states but we list only a small subset of the nondiagonal matrix elements in Table A.1. The second-order Breit–Coulomb corrections are relatively large and, therefore, must be included in accurate calculations. The nondiagonal matrix elements listed in the columns headed $E_2^{(2)}$ and $B_2^{(2)}$ are comparable with diagonal two-body matrix elements. However, the one-body contributions, $E_1^{(2)}$ and $B_1^{(2)}$, are larger than the corresponding two-body contributions, $E_2^{(2)}$ and $B_2^{(2)}$. As a result, the net second-order diagonal matrix elements are larger than the nondiagonal matrix elements in Table A.2.

In Table A.2, we present results for the Coulomb contributions, $E^{(0)}$, $E^{(1)}$, and $E^{(2)}$, and the Breit–Coulomb corrections, $B^{(1)}$ and $B^{(2)}$ obtained before diagonalization. Corrections for the frequency dependence of the Breit interaction [24] are included in the first order only. The difference between first-order Breit–Coulomb corrections calculated with and without frequency dependence is less than 1%. As one sees from Table A.2, the ratio of nondiagonal and diagonal matrix elements is larger for first-order contributions than for second-order contributions. Another difference in first- and second-order contributions is symmetry properties: first-order nondiagonal matrix elements are symmetric while the second-order nondiagonal matrix elements are not. $E^{(2)}(a'v'[J], av[J])$ and $E^{(2)}(av[J], a'v'[J])$ differ in some cases by factors of 2–3 and occasionally have opposite signs.

To determine the first-order energies of the states under consideration, we diagonalize the symmetric first-order effective Hamiltonian, including both the Coulomb and Breit interactions. The first-order expansion coefficient $C^N(av[J])$ is the Nth eigenvector of the first-order effective Hamiltonian and $E^{(1)}[N]$ is the corresponding eigenvalue. The resulting eigenvectors are used to evaluate the second-order Coulomb correction $E^{(2)}[N]$ as well as the second-order Breit–Coulomb correction $B^{(2)}[N]$.

In Table A.3, we list the following contributions to the energies of 15 excited states in Xe^{+8}: the sum of the zeroth and first-order energies $E^{(0+1)} = E^{(0)} + E^{(1)} + B_{\rm hf}^{(1)}$, the second-order Coulomb energy $E^{(2)}$, the second-order Breit–Coulomb correction $B^{(2)}$, and the sum of the above contributions $E_{\rm tot}$.

Table A.1. Second-order contributions to energy matrices (a.u.) for odd-parity states with $J = 1$ in Pd-like xenon, $Z = 54$. One-body and two-body second-order Coulomb and Breit–Coulomb contributions are given in columns labeled $E_1^{(2)}$, $E_2^{(2)}$, $B_1^{(2)}$, and $B_2^{(2)}$, respectively.

$4d_{j_1}\, nl_{2}\, j_2$	$4l_3\, j_3\, n'l_4\, j_4$	$E_1^{(2)}$	$E_2^{(2)}$	$B_1^{(2)}$	$B_2^{(2)}$
$4d_j 4f_{j'}$ [1] + $4d_j 5f_{j'}$ [1] states					
$4d_{5/2}4f_{5/2}$	$4d_{5/2}4f_{5/2}$	−0.112 309	0.073 927	0.007 163	0.000 856
$4d_{5/2}4f_{7/2}$	$4d_{5/2}4f_{7/2}$	−0.110 820	−0.024 173	0.007 267	0.000 255
$4d_{3/2}4f_{5/2}$	$4d_{3/2}4f_{5/2}$	−0.114 133	0.006 638	0.007272	0.000 509
$4d_{5/2}5f_{5/2}$	$4d_{5/2}5f_{5/2}$	−0.054 365	−0.032 374	0.010 636	0.000 140
$4d_{5/2}5f_{7/2}$	$4d_{5/2}5f_{7/2}$	−0.054 092	−0.017 309	0.010 650	0.000 085
$4d_{3/2}5f_{5/2}$	$4d_{3/2}5f_{5/2}$	−0.056 189	−0.020 837	0.010 745	0.000 144
$4d_{5/2}4f_{7/2}$	$4d_{3/2}4f_{5/2}$	0	0.086 037	0	0.000 462
$4d_{3/2}4f_{5/2}$	$4d_{5/2}4f_{7/2}$	0	0.086 871	0	0.000 441
$4d_{5/2}4f_{5/2}$	$4d_{5/2}5f_{7/2}$	0	0.022 362	0	0.000 307
$4d_{5/2}5f_{7/2}$	$4d_{5/2}4f_{5/2}$	0	−0.040 251	0	−0.000 422
$4d_j 5p_{j'}$ [1]+$4d_j 6p_{j'}$ [1] states					
$4d_{3/2}5p_{3/2}$	$4d_{3/2}5p_{3/2}$	−0.090 867	0.023 576	0.010 131	0.000 597
$4d_{3/2}5p_{1/2}$	$4d_{3/2}5p_{1/2}$	−0.095 575	0.025 054	0.010 004	0.000 727
$4d_{5/2}5p_{3/2}$	$4d_{5/2}5p_{3/2}$	−0.089 043	0.022 102	0.010 022	0.000 531
$4d_{3/2}6p_{3/2}$	$4d_{3/2}6p_{3/2}$	−0.048 985	−0.012 761	0.011 453	0.000 256
$4d_{3/2}6p_{1/2}$	$4d_{3/2}6p_{1/2}$	−0.050 015	−0.008 980	0.011 427	0.000 323
$4d_{5/2}6p_{3/2}$	$4d_{5/2}6p_{3/2}$	−0.047 160	−0.010 888	0.011 345	0.000 235
$4d_{3/2}5p_{3/2}$	$4d_{3/2}6p_{3/2}$	0	0.008 101	0	0.000 037
$4d_{3/2}6p_{3/2}$	$4d_{3/2}5p_{3/2}$	0	−0.000 260	0	0.000 491
$4d_{5/2}6p_{3/2}$	$4d_{3/2}5p_{3/2}$	0	−0.004 177	0	0.000 085
$4d_{3/2}5p_{1/2}$	$4d_{5/2}5p_{3/2}$	0	0.000 672	0	0.000 050

Table A.2. Diagonal and nondiagonal contributions to the energy matrix (a.u.). These contributions are listed for a odd-parity hole–particle states with $J = 1$ in Pd-like xenon, $Z = 54$.

		$E^{(0)}$	$E^{(1)}$	$B_{\rm hf}^{(1)}$	$E^{(2)}$	$B^{(2)}$
$4d_j 4f_{j'}$ [1]+$4d_j 5f_{j'}$ [1] states						
$4d_{5/2}4f_{5/2}$	$4d_{5/2}4f_{5/2}$	4.002 727	−0.851 736	−0.005 658	−0.038 381	0.008 019
$4d_{5/2}4f_{7/2}$	$4d_{5/2}4f_{7/2}$	4.004 396	−0.411 782	−0.006 227	−0.134 993	0.007 522
$4d_{3/2}4f_{5/2}$	$4d_{3/2}4f_{5/2}$	4.082 366	−0.535 663	−0.008 069	−0.107 495	0.007 781
$4d_{5/2}5f_{5/2}$	$4d_{5/2}5f_{5/2}$	5.011 411	−0.441 221	−0.006 660	−0.086 739	0.010 777
$4d_{5/2}5f_{7/2}$	$4d_{5/2}5f_{7/2}$	5.010 231	−0.352 094	−0.006 814	−0.071 401	0.010 734
$4d_{3/2}5f_{5/2}$	$4d_{3/2}5f_{5/2}$	5.091 050	−0.375 533	−0.008 909	−0.077 026	0.010 889
$4d_{5/2}4f_{7/2}$	$4d_{3/2}4f_{5/2}$	0	−0.390 363	0.000 198	0.086 037	0.000 462
$4d_{3/2}4f_{5/2}$	$4d_{5/2}4f_{7/2}$	0	−0.390 363	0.000 198	0.086 871	0.000 441
$4d_{5/2}4f_{5/2}$	$4d_{5/2}5f_{5/2}$	0	0.196 436	−0.000 054	−0.020 582	0.000 553
$4d_{5/2}5f_{5/2}$	$4d_{5/2}4f_{5/2}$	0	0.196 436	−0.000 054	0.000 836	−0.001 032

Table A.2. (*Concluded.*)

		$E^{(0)}$	$E^{(1)}$	$B^{(1)}_{\rm hf}$	$E^{(2)}$	$B^{(2)}$
$4d_j5p_{j'}$ [1]+$4d_j6p_{j'}$ [1] states						
$4d_{3/2}5p_{3/2}$	$4d_{3/2}5p_{3/2}$	3.465 775	−0.606 582	−0.006 781	−0.067 291	0.010 728
$4d_{3/2}5p_{1/2}$	$4d_{3/2}5p_{1/2}$	3.383 917	−0.591 982	−0.005 648	−0.070 521	0.010 731
$4d_{5/2}5p_{3/2}$	$4d_{5/2}5p_{3/2}$	3.386 136	−0.588 964	−0.004 578	−0.066 941	0.010 553
$4d_{3/2}6p_{3/2}$	$4d_{3/2}6p_{3/2}$	4.870 283	−0.369 668	−0.008 334	−0.061 745	0.011 710
$4d_{3/2}6p_{1/2}$	$4d_{3/2}6p_{1/2}$	4.836 995	−0.366 928	−0.007 893	−0.058 995	0.011 750
$4d_{5/2}6p_{3/2}$	$4d_{5/2}6p_{3/2}$	4.790 643	−0.365 499	−0.006 115	−0.058 048	0.011 580
$4d_{3/2}5p_{3/2}$	$4d_{3/2}6p_{3/2}$	0	−0.122 309	0.000 006	0.008 101	0.000 037
$4d_{3/2}6p_{3/2}$	$4d_{3/2}5p_{3/2}$	0	−0.122 309	0.000 006	−0.000 260	0.000 491
$4d_{5/2}6p_{3/2}$	$4d_{3/2}5p_{3/2}$	0	0.013 930	0.000 007	−0.004 177	0.000 085
$4d_{3/2}5p_{1/2}$	$4d_{5/2}5p_{3/2}$	0	−0.016 847	0.000 038	0.000 672	0.000 050

Table A.3. Energies (cm^{-1}) of odd-parity states with $J = 1$ relative to the ground state in the case of Pd-like xenon, $Z = 54$. $E^{(0+1)} \equiv E^{(0)} + E^{(1)} + B^{(1)}_{\rm hf}$.

Level-jj	Level-LS	$E^{(0+1)}$	$E^{(2)}$	$B^{(2)}$	$E_{\rm tot}$
$4d_{5/2}4f_{5/2}$	$4d4f\ ^3P_1$	667 834	−10 251	1 775	659 358
$4d_{5/2}4f_{7/2}$	$4d4f\ ^3D_1$	701 081	−7 805	1 799	695 075
$4d_{3/2}4f_{5/2}$	$4d4f\ ^1P_1$	865 559	−40 484	1 633	826 708
$4d_{5/2}5f_{5/2}$	$4d5f\ ^3P_1$	1 005 954	−17 983	2 338	990 309
$4d_{5/2}5f_{7/2}$	$4d5f\ ^3D_1$	1 016 961	−20 794	2 340	998 506
$4d_{3/2}5f_{5/2}$	$4d5f\ ^1P_1$	1 052 759	−15 939	2 344	1 039 164
$4d_{3/2}5p_{3/2}$	$4d5p\ ^3P_1$	603 083	−14 790	2 352	590 645
$4d_{3/2}5p_{1/2}$	$4d5p\ ^1P_1$	614 480	−15 022	2 333	601 792
$4d_{5/2}5p_{3/2}$	$4d5p\ ^3D_1$	627 641	−14 591	2 368	615 418
$4d_{3/2}6p_{3/2}$	$4d6p\ ^3P_1$	971 260	−12 843	2 534	960 950
$4d_{3/2}6p_{1/2}$	$4d6p\ ^1P_1$	980 603	−13 000	2 568	970 171
$4d_{5/2}6p_{3/2}$	$4d6p\ ^3D_1$	988 529	−13 931	2 561	977 159

Appendix B. E1 matrix elements for Xe^{+8}

In Table B.1, we list values of *uncoupled* first- and second-order E1 matrix elements $Z^{(1)}$, $Z^{(2)}$, $B^{(2)}$, together with derivative terms $P^{(\rm deriv)}$ for the 12 E1 transitions between odd-parity $J = 1$ states with and the ground state in Pd-like xenon, $Z = 54$. Matrix elements are given in both length (L) and velocity (V) forms. We see that the first-order matrix elements, $Z^{(1)}_L$ and $Z^{(1)}_V$, differ by 20–30% and the $L - V$ differences between second-order matrix elements are much larger for some transitions. The large differences in first- plus second-order matrix elements disappear after coupling.

Values of *coupled* E1 matrix elements in length and velocity forms are given in Table B.2 for the transitions considered in Table B.1. The first two columns in Table B.2 show the L and V values of the reduced matrix elements calculated in first order. The $L - V$ difference is about 20–25%. If we include the second-order contributions (columns headed First + Second order in Table B.2) the $L - V$ difference decreases to 3–4%. This large $L - V$ difference in the lowest order calculation arises because we start our MBPT calculations using a nonlocal DHF potential. If we were to replace the DHF potential by a local potential, the differences would disappear completely. It should be emphasized that we include negative energy state (NES) contributions to sums over intermediate states (see ref. 17 for details). Neglecting

Table B.1. Uncoupled reduced matrix elements in length L and velocity V forms for transitions from odd-parity states with $J = 1$ into the ground state in Xe^{+8}.

$av[J]$	$Z_L^{(1)}$	$Z_V^{(1)}$	$Z_L^{(2)}$	$Z_V^{(2)}$	$B_L^{(2)}$	$B_V^{(2)}$	$P_L^{(\mathrm{deriv})}$	$P_V^{(\mathrm{deriv})}$
$4d_{5/2}4f_{5/2}[1]$	−0.355 034	−0.276 197	0.046 114	−0.023 046	−0.000 152	0.000 407	−0.355 039	−0.000 125
$4d_{5/2}4f_{7/2}[1]$	1.587 063	1.236 167	−0.215 121	0.094 093	0.001 007	−0.001 359	1.586 495	−0.000 624
$4d_{3/2}4f_{5/2}[1]$	1.311 071	1.024 024	−0.181 366	0.074 495	0.001 042	−0.001 473	1.310 734	−0.000 241
$4d_{5/2}5f_{5/2}[1]$	−0.084 623	−0.063 932	0.016 209	−0.007 417	−0.000 108	0.000 059	−0.084 661	−0.000 053
$4d_{5/2}5f_{7/2}[1]$	0.381 899	0.289 004	−0.073 331	0.032 624	0.000 189	−0.000 396	0.381 889	−0.000 119
$4d_{3/2}5f_{5/2}[1]$	0.323 203	0.245 750	−0.062 910	0.026 535	0.000 361	−0.000 330	0.323 232	−0.000 017
$4d_{3/2}5p_{3/2}[1]$	−0.602 369	−0.459 228	0.031 482	−0.003 936	−0.000 571	0.000 312	−0.602 254	−0.000 063
$4d_{3/2}5p_{1/2}[1]$	0.471 485	0.360 397	−0.072 135	−0.035 844	0.000 278	−0.000 523	0.471 361	−0.000 033
$4d_{5/2}5p_{3/2}[1]$	−0.192 146	−0.147 879	0.004 731	−0.004 808	−0.000 226	0.000 154	−0.192 062	0.000 069
$4d_{3/2}6p_{3/2}[1]$	−0.214 308	−0.167 094	−0.074 938	−0.073 807	0.000 059	0.000 359	−0.214 288	−0.000 049
$4d_{3/2}6p_{1/2}[1]$	−0.163 207	−0.127 896	−0.059 201	−0.057 414	−0.000 052	0.000 263	−0.163 176	0.000 002
$4d_{5/2}6p_{3/2}[1]$	−0.069 267	−0.054 494	−0.021 644	−0.021 551	−0.000 065	0.000 072	−0.069 237	0.000 029

Table B.2. Coupled reduced matrix elements in length L and velocity V forms for transitions from odd-parity states with $J = 1$ to the ground state in Xe^{+8}.

	First order		First + Second order	
$av[J]$	L	V	L	V
$4d4f\,^3P_1$	−0.040 259	−0.030 620	−0.034 381	−0.033 315
$4d4f\,^3D_1$	0.094 469	0.071 445	0.086 029	0.082 300
$4d4f\,^1P_1$	1.950 059	1.522 731	1.689 214	1.649 958
$4d5f\,^3P_1$	0.034 392	0.026 473	0.029 157	0.027 995
$4d5f\,^3D_1$	−0.221 525	−0.169 910	−0.186 553	−0.179 215
$4d5f\,^1P_1$	0.870 436	0.668 357	0.727 942	0.701 366
$4d5p\,^3P_1$	−0.001 250	0.000 244	−0.037 850	−0.028 815
$4d5p\,^1P_1$	0.748 234	0.571 264	0.670 136	0.676 280
$4d5p\,^3D_1$	−0.293 622	−0.225 074	−0.296 226	−0.291 124
$4d6p\,^3P_1$	−0.159 274	−0.124 664	−0.232 483	−0.213 014
$4d6p\,^1P_1$	0.161 649	0.127 249	0.240 488	0.220 414
$4d6p\,^3D_1$	−0.043 139	−0.034 031	−0.059 278	−0.054 801

the NES contributions leads to small changes in the L-form matrix elements but to substantial changes in some of the V-form matrix elements with a consequent loss of form independence.

Appendix C. The second-order hole–particle contribution

To understand the irregularities in Fig. 3, we consider the second-order hole–particle contribution to the valence energy $E_v^{(2)}$ (eq. (2.6) in ref. 6) and to the interaction energy $E^{R_3}(a'v'[J], av[J])$ (eq. (2.10) in ref. 6). A typical double-excitation contribution to the valence energy has the form [6]

$$A(v) \propto \sum_{mnc} \sum_{l} \frac{X_l(vcmn)X_l(mncv)}{\epsilon_v + \epsilon_c - \epsilon_m - \epsilon_n} \tag{C.1}$$

where $X_l(vwmn)$ is the product of a Slater integral and angular momentum coefficients, ϵ_m and ϵ_n are zeroth-order one-particle energies, ϵ_c is a zeroth-order core orbital energy, and ϵ_v is the zeroth-order

valence orbital energy.

We found a sharp increase in the values of the second-order valence energy for $5f_{7/2}$ states ($Z = 79$) and $5f_{5/2}$ states ($Z = 89$). The denominator of one term in (C.1) $\epsilon_{5f_{7/2}} + \epsilon_{4d_{5/2}} - \epsilon_{5s_{1/2}} - \epsilon_{4f_{5/2}} = -0.0076$ occurs for $Z = 79$. Moreover, the denominator of another term $\epsilon_{5f_{5/2}} + \epsilon_{4d_{3/2}} - \epsilon_{4f_{7/2}} - \epsilon_{5s_{1/2}} = -0.0099$ occurs for $Z = 89$. These small denominators lead to the increases in $A(5f_{7/2})$ and $A(5f_{5/2})$ by factors of 3–5, leading in turn to sharp deviations from smooth curves in Fig. 3 for $Z = 79$ and 89.

Two terms in $E^{R_3}(a'v'[J], av[J])$ are responsible for sharp features in the curves shown in Fig. 3 for $Z = 64$ and $Z = 81$. The first term is [6]

$$E_1^{R_3}(a'v'[J], av[J]) \propto \sum_{nc} \frac{Z_J(vcan)Z_J(a'nv'c)}{\epsilon_v + \epsilon_c - \epsilon_n - \epsilon_a} \tag{C.2}$$

where $Z_J(vcan)$ is a symmetrized Coulomb integral (see ref. 6). We found an increase (by a factor of 2) in the contribution from (C.2) for $Z = 64$. In this case, the denominator is $\epsilon_{5f_{7/2}} + \epsilon_{4p_{3/2}} - \epsilon_{5s_{1/2}} - \epsilon_{4d_{5/2}} = -0.00746$, leading to the sharp feature at $Z = 64$ in Fig. 3 The second term is [6]

$$E_2^{R_3}(a'v'[J], av[J]) \propto \sum_{nc} \frac{Z_J(vcv'n)Z_J(a'nac)}{\epsilon_v + \epsilon_c - \epsilon_n - \epsilon_{v'}} \tag{C.3}$$

We also found a factor 2 increase in the contribution from (C.3) for $Z = 81$. In this case, the denominator is $\epsilon_{5f_{7/2}} + \epsilon_{4p_{3/2}} - \epsilon_{4f_{7/2}} - \epsilon_{4f_{7/2}} = 0.0069$, leading to the sharp feature in Fig. 3 at $Z = 81$.

Appendix D. The second-order dipole matrix element

A typical contribution from one of the second-order reduced matrix elements $Z_1^{(\mathrm{RPA})}[0 - av[1]]$ has the form [6]

$$Z_1^{(\mathrm{RPA})}(0 - av[1]) \propto \sum_{b,i} \frac{Z_1(bi)Z_1(aivb)}{\varepsilon_b + \varepsilon_v - \varepsilon_i - \varepsilon_a} \tag{D.1}$$

The one-electron electric-dipole matrix element $Z_1(bi)$, defined in ref. 17 includes retardation and is calculated in length and velocity forms. In the sum over i, only terms with vanishing denominators are excluded. We found the sharp increase (by a factor of 2–5) in values of the $Z_1^{(\mathrm{RPA})}(0 - av[1])$ contributions for $Z = 57$ ($av = 4d_{3/2}6p_{1/2}$) and for $Z = 61$, 67, and 79 ($av = 4d_{5/2}6p_{3/2}$) by resulting from very small values of the denominator D in (D.1).

(*i*) $av = 4d_{3/2}6p_{1/2}, \quad Z = 57$

$$D = \epsilon_{4d_{5/2}} + \epsilon_{6p_{1/2}} - \epsilon_{5f_{7/2}} - \epsilon_{4d_{3/2}} = -10.1802 - 3.1639 + 3.0443 + 10.2988 = -0.0010$$

(*ii*) $av = 4d_{5/2}6p_{3/2}, \quad Z = 61$

$$D = \epsilon_{4p_{3/2}} + \epsilon_{6p_{3/2}} - \epsilon_{5s_{1/2}} - \epsilon_{4d_{5/2}} = -20.4963 - 5.2512 + 9.8620 + 15.8751 = -0.0104$$

(*iii*) $av = 4d_{5/2}6p_{3/2}, \quad Z = 67$

$$D = \epsilon_{4p_{1/2}} + \epsilon_{6p_{3/2}} - \epsilon_{5s_{1/2}} - \epsilon_{4d_{5/2}} = -33.8633 - 9.3802 + 16.8595 + 26.3713 = -0.0127$$

(*iv*) $av = 4d_{5/2}6p_{3/2}, \quad Z = 79$

$$D = \epsilon_{4p_{3/2}} + \epsilon_{6p_{3/2}} - \epsilon_{5d_{5/2}} - \epsilon_{4d_{5/2}} = -62.6012 - 20.8374 + 29.1876 + 54.2837 = 0.0327$$